Structure and dynamics of the kinase IKK-β – a key regulator of the NF-kappa B transcription factor

Munishikha Kalia[a,b], Andreas Kukol[a*]

[a] School of Life Sciences, University of Hertfordshire, Hatfield AL10 9AB, United Kingdom

[b] Current address: Institut für Molekulare Medizin, Universität zu Lübeck, D-23562 Lübeck, Germany

* Corresponding author: a.kukol@herts.ac.uk, Tel.: +44(0)1707 284543, fax: +44(0)1707 284870

ABSTRACT

The inhibitor κB kinase-β (IKK-β) phosphorylates the NF-κB inhibitor protein IκB leading to the translocation of the transcription factor NF-κB to the nucleus. The transcription factor NF-κB and consequently IKK-β are central to signal transduction pathways of mammalian cells. The purpose of this research was to develop a 3D structural model of the IKK-β kinase domain with its ATP cofactor and investigate its dynamics and ligand binding potential. Through a combination of comparative modelling and simulated heating/annealing molecular dynamics (SAMD) simulation in explicit water the model accuracy could be substantially improved compared to comparative modelling on its own as shown by model validation measures. The structure revealed the details of ATP/Mg^{2+} binding indicating hydrophobic interactions with the adenine base and a significant contribution of Mg^{2+} as a bridge between ATP phosphate groups and negatively charged side chains. The molecular dynamics trajectories of the ATP-bound and free enzyme showed two conformations in each case, which contributed to the majority of the trajectory. The ATP-free enzyme revealed a novel binding site distant from the ATP binding site that was not encountered in the ATP bound enzyme. Based on the overall structural flexibility, it is suggested that a truncated version of the kinase domain from Ala14 to Leu265 should be subjected to crystallisation trials.
The 3D structure of this enzyme will enable rational design of new ligands and analysis of protein-protein interactions. Furthermore, our results may provide a new impetus for wet-lab based structural investigation focussing on a truncated kinase domain.

Keywords: protein kinase, protein structure, comparative modelling, molecular dynamics, binding site

Introduction

The inhibitor κB kinase-β (IKK-β, IKBKB, IKK2) is a key enzyme in the activation pathway of the transcription factor NF-κB. IKK-β phosphorylates the NF-κB inhibitor protein IκB leading to its ubiquitinylation and degradation as reviewed by Schmid & Birbach (2008). NF-κb is then translocated to the nucleus, where it stimulates the transcription of genes. IKK-β and subsequent NF-κB activation occurs due to a variety of inflammatory stimuli including viral and bacterial pathogens (Chu et al., 1999). Changes in IKK-β regulation have also been linked to various forms of cancer (Bollrath and Greten, 2009; Hernandez et al., 2010; Karin and Greten, 2005), heart disease (Gupta et al., 2008; Konia et al., 2009) and to the development of type II diabetes (Arkan et al., 2005). Recently IKK-β has been characterised as a novel drug target against influenza virus infection. The known low affinity inhibitor aspirin (Yin et al., 1998) was shown to protect mice from influenza infection, when inhaled prior to virus exposure, and, most importantly, it did not induce virus resistance in multi-passaging experiments (Mazur et al., 2007). The high mutation rate of influenza virus proteins causing the development of resistance against the existing M2 proton channel inhibitors (Barr et al., 2008; Barr et al., 2007) and neuraminidase inhibitors (Handel et al., 2007; Yen et al., 2006) lead to the proposal of IKK-β as novel drug target of the host cell against influenza infection (Ludwig and Planz, 2008).

IKK-β exists as part of a complex consisting of two catalytic subunits, IKK-α (also known as IKK1), IKK-β and a regulatory subunit IKK-γ (NEMO); they predominantly exist as IKK-α/IKK-β heterodimer associated with IKK-γ (Krappmann et al., 2000). Although IKK-α and IKK-β have overall 52% sequence identity and >70% homology (Burke and Strnad, 2002; Woronicz et al., 1997), IKK-β is the essential enzyme for phosphorylation of IκB (Delhase et al., 1999), since cells lacking IKK-α show normal induction of NF-κB DNA-binding activity in response to most stimuli and pathogens (Chu et al., 1999; Delhase et al., 1999).

The human IKK-β sequence is 756 amino acid residues long and has a molecular mass of 86.6 kDa (DiDonato et al., 1997; Woronicz et al., 1997). It consists of a kinase domain (residues 15-312), a leucine zipper domain (458-479), a helix-loop-helix domain (566-645) and the IKK-γ binding domain (734-744) (Mercurio et al., 1997). Activation of IKK-β requires phosphorylation of Ser177 and Ser181 (Lallena et al., 1999), and more recently Tyr188 and Tyr199 were identified as necessary for activation (Darwech et al., 2010a; Huang

et al., 2003), while the phosphatases PPM1A and PPM1B play a role in deactivation (Sun et al., 2009).

Despite the pronounced interest into IKK-β as a drug target, because of its central role in a key signal transduction pathway, no experimental 3D structure is available. However, some models of the kinase domain based on comparative modelling have been published (Avila et al., 2009; Lauria et al., 2010; Mathialagan et al., 2010; Nagarajan et al.), but the 3D structures are not available either in public databases or from the authors of the studies. It appears that in most of these studies straightforward comparative modelling using the BLAST algorithm for template selection and the automated Modeller (Eswar et al., 2008) or the Swiss-Model (Guex et al., 2009) server was used for model building. Crucially, the co-factor ATP normally located in the active site was not included in most studies, apart from the study by Avila et al. (Avila et al., 2009), which developed a comparative model based on one template with the 'first approach mode' of the Swiss-Model server. It has been suggested that comparative models, which include the natural ligand, can lead to similar and in some cases to better results for protein-ligand docking, than crystal structures without the ligand (Rockey and Elcock, 2006).

In this study we report the comparative model of the IKK-β kinase domain based on multiple templates including the ATP co-factor and Mg^{2+} ions. The resulting model was refined through molecular dynamics (MD) simulations using a simulated heating/annealing protocol in an explicit water environment. Our results reveal model accuracy, which is superior to some of the structural templates used in terms of model assessment parameters. In order to identify small-scale conformational changes and novel allosteric binding sites the model was subjected to constant temperature MD simulations over 80 ns. While simulations of this time scale are too short to reveal large conformational changes or even protein folding events, it was shown that this time scale is sufficient to explore the conformation of loops and side-chains in agreement with experimental data (Almond et al., 2007; Nederveen and Bonvin, 2005). Our results reveal the molecular details of ATP and peptide substrate ligand binding, the role of the activation loop and conformational changes. This study will facilitate virtual screening and rational drug design efforts for this biomedically important protein kinase.

Materials and methods

The computations were performed on a dual-socket dual-core AMD Opteron workstation (Digital Networks UK, Hyde) and a cluster build from 80 two-socket quad core Intel Xeon E5520 nodes (Dell Inc., USA).

Template selection and alignment

The primary sequence of human IKK-β was retrieved from UniProtKB (Apweiler et al., 2010; Jain et al., 2009) (http://www.uniprot.org/) under the accession number `014920`. The IKK-β kinase domain ranging from 1-300 amino acid residues was used to identify homologous sequences by Hidden Markov Model Comparison using the HHpred (Hildebrand et al., 2009) web server (http://toolkit.tuebingen.mpg.de/hhpred) searching against the pdb70 database with a maximum of eight PSI-BLAST iterations including the scoring of secondary structure and a local alignment mode. Five templates were chosen, *viz* 3G51A, 3FE3A, 3HKOA, 3DTCA & 1ZY4A based on high sequence identity between 29% and 31%. An additional template (1PHKA) with a lower sequence identity of 27% was selected that covered any stretches of the target sequence that had no matches with the previous five templates in order to avoid the process of loop modelling. Another template (1RDQE) with 27% sequence identity was selected that had ATP and Mg^{2+} as cofactors. The query sequence and template sequences were further aligned by 'SALIGN' program of the Modeller9v7 (Fiser and Sali, 2003; Sali and Blundell, 1993) software with an rms_cutoff=3.5, gap_penalties_1d=(-450, -50), gap_penalties_3d=(0,3) and the alignment_type='progressive'.

Homology modelling and model assessment

The homology model of the IKK-β kinase domain was generated by the Modeler9v7 (Fiser and Sali, 2003; Sali and Blundell, 1993) program using the cofactors ATP and Mg^{2+} during the modelling process. Initially 100 models were generated, with a thorough optimisation using the variable target function method (automodel.library_schedule = autosched.slow) with a maximum number of conjugate gradient iterations of 300, followed by a slow refinement with simulated annealing molecular dynamics (automodel.md_level = refine.slow).

Initially the models were assessed based on the normalised Discrete Optimized Protein Energy (Shen and Sali, 2006) (DOPE) scores. Ten models with the lowest DOPE score were selected and further rated with MolProbity (Chen et al., 2010). The MolProbity score was highlighted as a good measure of the protein-likeliness in an analysis of all-atom accuracy of models from the Critical Assessment of Protein Structure Prediction (CASP8) exercise (Keedy et al., 2009). The model with the lowest MolProbity score and suitable peptide

backbone dihedral angles as reported by by Ramachandran plot analysis (Lovell et al., 2003) was selected.
An all-atom model was generated by adding hydrogen atoms with the HAAD algorithm (Li et al., 2009), which was reported to have a higher accuracy than the widely used program REDUCE (Word et al., 1999).

System preparation
All the energy minimisations (EM) and molecular dynamics (MD) simulations were performed with the GROMACS 4.07 simulation package (Hess et al., 2008) employing the AMBER03 force field (Duan et al., 2003) ported to GROMACS (DePaul et al., 2010; Sorin and Pande, 2005). AMBER03 is a variant of the AMBER99 force field, which was successfully used for many all-atom protein MD simulations (Cerutti et al., 2010; Ponder and Case, 2003). The standard AMBER building blocks were used to build the topology, except for ATP. The atomic charges of ATP^{3-} were obtained with the RESP ESP Charge Derive (Dupradeau et al., 2010) and provided by François-Yves Dupradeau (personal communication). The AMBER topology for Gromacs was generated from the Tripos MOL2 format with the ACPYPE web portal (http://webapps.ccpn.ac.uk/acpype/) that includes Antechamber (Wang et al., 2006). The protein/ATP/Mg system was solvated with 9723 TIP3P water (Mahoney and Jorgensen, 2000) molecules and neutralised with one Na^+ ion that replaced a water molecule at the position of favourable electrostatic potential. The charges on the protein were chosen automatically in accordance with a pH of 7.0.
The energy of the system was minimised with 2000 steps of the conjugate gradient method, while keeping the protein and ATP heavy atoms restrained to their original positions. Lennard-Jones interactions were calculated with a cut-off of 1.4nm, while electrostatic interactions were treated with the Particle-Mesh-Ewald method using a real space cut-off of 1.0 nm.
In the next step 500 ps of MD simulations with position restraints on the protein and ATP non-hydrogen atoms were performed. A time step of 2 fs was used at a temperature of 298K, kept constant via a stochastic velocity rescaling thermostat (Bussi et al., 2009) using a coupling constant of 1.0 ps. Isotropic Berendsen pressure coupling (Berendsen et al., 1984) with a time constant of 1.0 ps was applied to keep the pressure constant at 1.0 bar. Covalent bonds of the protein and the ATP were constrained with the LINCS algorithm (Hess et al., 1997), while water molecules were constrained with the SETTLE algorithm (Miyamoto and Kollman, 1992). Long-range dispersion corrections for energy and pressure were applied.

After a further 2000 steps of conjugate gradient energy minimization without any position restraints the system was subjected to unrestrained MD simulations.

Simulated heating/annealing MD (SAMD)

SAMD of the unrestrained system was performed, by heating from 20K to 280K over a period of 4000 ps and annealing from 280K to 20K for another 4000 ps. All other parameters were as described above. Afterwards the system was subjected to 2000 steps of conjugate gradient energy minimization. The same SAMD/EM protocol was repeated twenty times with different random initial atom velocities. The ensemble of twenty structures was analysed with respect to the root mean square deviation (RMSD) of the peptide backbone atom coordinates with the g_cluster program of the GROMACS 4.07 package. The **final SAMD model** was chosen as the central structure, i.e. the structure that was most similar to all other structures of the ensemble.

Constant temperature MD simulations

The final model with ATP/Mg^{2+} bound was subjected to MD simulation at a temperature of 298K over a period of 80 ns. All other parameters were as described above. For the MD simulation of the protein without ATP, the ATP/Mg coordinates were deleted and the system was subjected to 2000 steps of conjugate gradient energy minimisation followed by 500 ps of MD simulations with position restraints on the protein non-hydrogen atoms. After a further 2000 steps of energy minimisation the unrestrained MD simulation was run over a period of 80 ns. Tow repeat simulations for each system were run over a period of 50 ns.

The trajectory between 10 ns and 80 ns was analysed for clusters of similar structures using the g_cluster tool of the GROMACS software package with a cutoff of 0.3 nm and the Gromos clustering algorithm (Daura et al., 1999). The pdb-files of central cluster structures are available as supplementary material.

Binding site prediction

Binding sites of the final model were predicted by computational solvent docking, in which a library of small organic probe molecules was docked to the protein without ATP/Mg^{2+} using the FTmap algorithm (Brenke et al., 2009). It was shown that a cluster of probes found by FTmap can identify important subsites of a protein binding site and that a group of vicinal clusters can map out a protein binding site with high accuracy (Landon et al., 2009).

Accession numbers

The final model after the SAMD protocol was submitted to the Protein Model Database (Castrignano et al., 2006) and is available under the identifier PM0076858.

Results and discussion

Template identification & multiple sequence alignment

Templates were identified with HHpred (Hildebrand et al., 2009), which utilises the pairwise comparison of profile hidden Markow models that provides superior sensitivity and selectivity compared to sequence-profile based methods like PSI-BLAST. From almost 800 protein serine/theronine kinase structures available in the RCSB protein databank (Berman et al., 2000) the HHpred algorithm identified the best 100 structural templates with sequence identities ranging from18% to 31%. Five templates were chosen, namely 3G51A (31% sequence identity), 3FE3A (31% sequence identity), 3HKOA (30% sequence identity), 3DTCA (30% sequence identity) and 1ZY4A 29% sequence identity). Inaccuracies in comparative modelling can arise through large gaps (Lushington, 2008), where the target sequence is not covered by any structural template. In order to avoid these inaccuracies a further template 1PHK with 27% sequence identity was selected that covered all gaps in the alignment. For an accurate description of the ATP binding site it is necessary to include ATP in the modelling process, which was found in the template 1RDQE (27% sequence identity). The resulting structure/sequence alignment obtained from the Modeller SALIGN procedure is shown in figure 1(a) shaded according to similarity scores based on the BLOSSUM62 matrix (Henikoff and Henikoff, 1992). Except for the first eleven N-terminal residues there is a good coverage of the query sequence by at least one of the templates. Another region of low sequence similarity is in the C-terminal region 286-300 of the query sequence. The ATP binding site residues 21 to 29 is highly conserved; seven out of nine amino acid residues are identical between the query sequence and the template (1RDQE). The key residues lysine 44 and tyrosine 188/199 are conserved in most templates, while Ser 177/181 are matched with the template 1PHKA.

Modelling of IKK-β kinase domain

The 100 initial models generated by Modeller9v7 resulted in normalised Discrete Optimized Protein Energy (Shen and Sali, 2006) (DOPE) z-scores between -0.044 and -0.388. The ten models with the lowest DOPE-z scores were then further assessed with ‘MolProbity’. The MolProbity scores ranged from 3.08 to 3.87. The model with the lowest MolProbity score of

3.08, which had also the lowest DOPE z-score of -0.388, was selected for further refinement with SAMD simulations in the presence of explicit water and counter ions. The SAMD protocol was carried out 20 times. The maximum peptide backbone RMSD between the 20 structures was 1.86 Å and the structure, which was most similar to all other structures, was chosen as the final model. This model was assessed using DOPE z-scores, MolProbity and PROCHEK. The results in table 1 show that the DOPE z-scores of the model was improved by the SAMD simulation from -0.388 to -0.779, while the range of DOPE z-scores for the template structures obtained by x-ray crystallography are between -1.28 and -1.8. The scores of experimental structures are in all cases lower (better) than the initial model and the SAMD-refined model, while the SAMD method lead to an improved DOPE-z score compared to the initial model. As a further assessment the MolProbity score was calculated, which was reported as a full-model measure that correlates well with model accuracy using predicted structures in the recent Critical Assessment of protein structure Prediction (CASP8) exercise (Keedy et al., 2009). The MolProbity scores shown in table 1 are with one exception lower than the initial model as it would be expected. Most notably, the MolProbity score for the SAMD model of 0.98 is lower than any of the templates indicating that the SAMD protocol resulted in a marked increase of all-atom accuracy, which exceeds every template structure used.

The analysis of peptide backbone dihedral angles based on the Ramachandran plot (table 1) showed that experimental structures had a higher proportion of residues in the allowed regions, than both of the models with the exception of 3DTC. The differences were, however minor.

The comparison of the initial model with the SAMD model in figure 2a showed that the per-residue DOPE score was improved for every residue in the model except for the last three C-terminal residues. The most apparent structural differences were visible in the N-terminal α-helix up to residue Arg20, in the antiparallel β-sheet from His33 to Ile43, in a helix-loop-helix motif from Gln110 to Ile122, in the loop Gly156 to Arg159 and in a C-terminal disordered region starting from Gln278.

Overall the SAMD simulation resulted in a more compact well defined structure, which was significantly protein-like as evidenced by the MolProbity score.

IKK-β structure

The model for IKK-β showed the typical two-lobe structure (figure 3a) of eukaryotic serine/threonine and tyrosine protein kinases analysed by Hanks & Hunter (Hanks and

Hunter, 1995) with a C-terminal lobe rich in α-helices and an N-terminal lobe rich in β-sheet secondary structures. The deep cleft between the two lobes is the site of ATP binding, while the peptide substrate is known to bind to the C-lobe. The location of typical structural features reviewed by Huse and Kuriyan (2002) has been highlighted in figure 3a, such as the phosphate binding (P-) loop from Gly22 to Val29, the only α-helix in the N-lobe from Arg53 to Arg67 (αC helix) and the activation loop from Leu167 to Tyr188. The αC helix is known to undergo positional changes due to regulation of the kinase activity, e.g. in cyclin-dependent kinases (Debondt et al., 1993; Jeffrey et al., 1995), where the αC helix undergoes a rotation due to the binding of cyclin. The activation loop contains residues Ser177, Ser181 that are phosphorylated as part of the activation mechanism (Lallena et al., 1999) as well as Tyr188 and Tyr199 (Darwech et al., 2010b; Huang et al., 2003) with Tyr199 being outside the commonly known activation loop. In the model shown in figure 3a the activation loop points away from the ATP binding site, which is characteristic of the active form of the kinase, while in the inactive form the activation loop adopts a conformation that impedes the binding of ATP and the peptide substrate (Hubbard et al., 1994).
A long C-terminal segment from Leu265 to Phe300 is unstructured and remains unstructured in conformations encountered during molecular dynamics simulations (see below). .

ATP binding

The adenine base of the ATP molecule was mainly bound via hydrophobic contacts to the protein provided by Leu21, Gly22, Gly24, Val29, Ala42, Tyr98 and Ile165 (figure 3b and 3c). In addition the peptide backbone carbonyl oxygen of Glu97 acted as a hydrogen acceptor and the backbone NH of Cys99 as a hydrogen bond donor to the adenine base. The majority of hydrogen bond and electrostatic interactions occurred with the triphosphate group of ATP. Interestingly only one positively charged side chain of Lys147 contributed to the stabilisation of the terminal phosphate group, while Asp145 and Asp166 interact with the magnesium ions. The magnesium ions fulfilled a role as a bridge between the negatively charged phosphate oxygens and negatively charged side-chains of the protein. Furthermore, the backbone NH groups of Gly25, Phe26 and Gly27 act as hydrogen bond donors to phosphate terminal and bridging oxygen atoms. The highly conserved Lys44 interacted with the oxygen of the proximal phosphate group. Asp145 corresponds to a highly conserved Asp166 in protein kinase A that interacts with the hydroxyl side chain of the peptide substrate. The detailed analysis of the conformational dynamics (see below) shows that this residue is quite

flexible in our model, thus upon binding of the peptide substrate the orientation of the side-chain may switch into another conformation.

From this analysis some general features of new inhibitors can be devised. Potential inhibitors should have a significant number of hydrophobic centres that fit deeply into the ATP-binding cavity. In addition, both positively and negatively charged groups are required for interaction with Asp145/Asp146 on the one hand and Lys147/Lys44 on the other hand.

Conformational dynamics of IKK-β

The conformational dynamics at room temperature in the vicinity of the SAMD-refined comparative model was analysed by subjecting the IKK-β model with bound ATP (holo-enzyme) and without ATP (apo-enzyme) to 80 ns MD simulation. During both simulations the protein backbone underwent a substantial conformational change with respect to the starting structure as revealed by a root mean square deviation (RMSD) of the backbone coordinates of up to 0.6 nm as shown in figure 4. Similar trajectories were obtained in two 50 ns repeat simulations for each system (data not shown). There was a sharp increase of the RMSD from the starting structure during the first 5 to 6 ns to an RMSD of 0.4 nm; thereafter the increase in RMSD is less pronounced. Taking into consideration that the final model of the holo-enzyme was obtained through SAMD simulations and energy minimisation of the same system used for the constant temperature simulations shown here, the large RMSD reached over 80 ns is surprising. RMSDs of conformationally stable proteins remain within 0.2 to 0.3 nm of the experimental starting structure during MD simulations. The higher structural fluctuations shown in this study are indicative of the conformational flexibility of the protein, which would have a negative impact on crystallisation for x-ray structural analysis. Based on our observation of a long C-terminal segment that lacks secondary structure we recommend crystallisation of a reduced length kinase domain from Ala14 to Leu265.

Comparison of the trajectories of the protein with and without ATP (figure 4) shows that the RMSD values with respect to the starting structure are overall similar. During the first 5 ns there was a sharp increase in the RMSD for the apo-enzyme reflecting the structural adaption to the removal of ATP, but there was a tendency for the apo-enzyme to adopt lower RMSD values than the holo-enzyme. It should be noted, however, that the RMSD was calculated with respect to the beginning of the simulation. While the RMSD is indicative of the deviation of the simulation from the starting structure, the root mean square fluctuation (RMSF) can capture the equilibrium dynamics. In order to exclude the fluctuations at the

beginning of the simulation due to the removal of ATP for the apo-enzyme, the RMSF between 10 and 80 ns was calculated (figure 5). The average RMSF per residue shown in figure 5a revealed that the holo-enzyme structure was overall more stable than the structure of the apo-enzyme. Residues that showed a particular high structural fluctuation were 9, 83 and 114. The mapping of the RMSF onto the 3D structure using a colour gradient from blue (low RMSF) to red (high RMSF) revealed similarly that the holo-enzyme shows overall less fluctuations apart from a segment of the αC helix from Arg47 to Glu61, that was in contact with Pro88-Pro92, which showed also high RMSF values (figure 5b and c). The apo-enzyme showed fluctuations throughout the structure, but not in the aforementioned segments. It is, therefore, tempting to speculate that the high RMSF values in a few segments of the holo-enzyme indicate conformational fluctuations that bring ATP into close contact with the protein phosphorylation substrate. The same observations with regards to RMSF were made in repeated simulations (data not shown).

Given the high RMSD with respect to the starting structure for both apo- and holo-enzyme, it is clear that the final outcome of the comparative modelling process described above is not the major conformation of IKK-β in solution. A cluster analysis of the trajectory resulted in the identification of three conformations in case of holo-enzyme and four conformations in case of the apo-enzyme (table 2).

In both cases there were two predominant conformations, which were encountered in 74% of the trajectory for the holo-enzyme and in 83.5% of the trajectory for the apo-enzyme. These conformations were not identical, as the protein backbone RMSD between them was 0.55 nm. Visual comparison of these two conformations in figure 6a and 6b (leftmost structure) showed that there were subtle differences throughout the structure but most apparently in the orientation of an N-terminal segment and an anti-parallel beta-hairpin from Asp78 to Arg95, that does not show any beta-structure in the holo-enzyme. The two minor conformations showed similar differences, which were overall less pronounced resulting in an RMSD of 0.38 nm between ATP2 and noATP2. The overlay of all three or four conformations of the holo- and apo-enzyme respectively with the comparative model (figure 6, right hand side) showed that the holo-form underwent major structural changes in the N-lobe, while the structural changes in the C-lobe were more subtle. The apo-form showed significant structural changes throughout, which would be expected as the protein structure was modelled with the ATP cofactor bound.

It should be noted that the simulation time of 80 ns limits the conformational changes to small scale motions in the vicinity of the starting structure, which nevertheless allow the

exploration of side-chain movements and loop flexibility that is in agreement with NMR experiments (Almond et al., 2007) and may critically influence ligand binding.

Binding site prediction

Given the structural changes observed, we investigated, if the ATP binding site was retained in the apo-form and if other binding sites for potential allosteric modulators are available using computational solvent mapping (Brenke et al., 2009). Figure 7 shows the predicted binding sites for the two major conformations of the apo-enzyme. In the most populated conformation noATP1 (figure 7a) the ATP binding site is mapped out by clusters of solvent molecules ranked at place two and four. In the conformation noATP2 (figure 7b) the highest ranked binding sub-site one does not coincide with the original ATP binding site, while sub-site two retains the position shown in figure 7a. It is possible that the conformation noATP2 represents a pre-ATP binding state, which allows ATP interaction at sub-sites one and two followed by a conformational change that allows ATP to slip into its deep binding pocket. An additional highly ranked binding site of conformation noATP1 (figure 7a) was predicted by solvent clusters one and three at a location distant from ATP binding. This binding site is formed by the helix Thr200-Gly218 and residues Lys254/Ser258 from a short C-terminal helix. Pro260, Tyr261 and Asn263 also contribute to the binding site. The binding site was partially retained in the conformation noATP2, but based on lower ranked solvent clusters. Interestingly, this binding site was not seen in the ATP bound conformations (data not shown), thus it may be an allosteric binding site that could be targeted with ligands that lock IKK-β in an ATP-free inactive conformation. Another possibility for the design of novel inhibitors may be targeting the highly ranked sub-sites one and two in the pre-ATP conformation.

Conclusion

In the absence of a crystal- or NMR-structure of the IKK-β kinase, a comparative model was developed and it was demonstrated how the model accuracy can be improved by simulated annealing MD simulations. Importantly, the ATP co-factor was included in the modelling process, which renders the present structure an ideal starting point for receptor-based virtual screening efforts as well as rational drug-design. The location of structural elements and residues interacting with ATP is commensurate with the structural details of other Ser/Thr kinases known from x-ray crystallography confirming the accuracy of the present model. In

addition the conformational dynamics of the apo-form of the kinase showed the emergence of additional binding sites that could lead to the design of new isosteric as well as allosteric modulators.

Acknowledgements

We thank Ben Webb for help with the Modeller software, François-Yves Dupradeau for deriving the atomic charges of the ATP molecule and Martin Hardcastle for the set-up of a computer cluster including software installation. This work was funded by the School of Life Sciences at the Health and Human Sciences Research Institute, University of Hertfordshire, Hatfield, United Kingdom.

REFERENCES

Almond, A., C.D. Blundell, V.A. Higman, A.D. MacKerell, and A.J. Day, 2007. Using molecular dynamics simulations to provide new insights into protein structure on the nanosecond timescale: Comparison with experimental data and biological inferences for the hyaluronan-binding link module of TSG-6. Journal of Chemical Theory and Computation 3: 1-16.

Apweiler, R., M.J. Martin, C. O'Donovan, M. Magrane, Y. Alam-Faruque, R. Antunes, D. Barrell, B. Bely, M. Bingley, D. Binns, L. Bower, P. Browne, W.M. Chan, E. Dimmer, R. Eberhardt, A. Fedotov, R. Foulger, J. Garavelli, R. Huntley, J. Jacobsen, M. Kleen, K. Laiho, R. Leinonen, D. Legge, Q. Lin, W.D. Liu, J. Luo, S. Orchard, S. Patient, D. Poggioli, M. Pruess, M. Corbett, G. di Martino, M. Donnelly, P. van Rensburg, A. Bairoch, L. Bougueleret, I. Xenarios, S. Altairac, A. Auchincloss, G. Argoud-Puy, K. Axelsen, D. Baratin, M.C. Blatter, B. Boeckmann, J. Bolleman, L. Bollondi, E. Boutet, S.B. Quintaje, L. Breuza, A. Bridge, E. deCastro, L. Ciapina, D. Coral, E. Coudert, I. Cusin, G. Delbard, M. Doche, D. Dornevil, P.D. Roggli, S. Duvaud, A. Estreicher, L. Famiglietti, M. Feuermann, S. Gehant, N. Farriol-Mathis, S. Ferro, E. Gasteiger, A. Gateau, V. Gerritsen, A. Gos, N. Gruaz-Gumowski, U. Hinz, C. Hulo, N. Hulo, J. James, S. Jimenez, F. Jungo, T. Kappler, G. Keller, C. Lachaize, L. Lane-Guermonprez, P. Langendijk-Genevaux, V. Lara, P. Lemercier, D. Lieberherr, T.D. Lima, V. Mangold, X. Martin, P. Masson, M. Moinat, A. Morgat, A. Mottaz, S. Paesano, I. Pedruzzi, S. Pilbout, V. Pillet, S. Poux, M. Pozzato, N. Redaschi*, et al.*, 2010. The Universal Protein Resource (UniProt) in 2010. Nucleic Acids Research 38: D142-D148.

Arkan, M.C., A.L. Hevener, F.R. Greten, S. Maeda, Z.W. Li, J.M. Long, A. Wynshaw-Boris, G. Poli, J. Olefsky, and M. Karin, 2005. IKK-beta links inflammation to obesity-induced insulin resistance. Nature Medicine 11: 191-198.

Avila, C.M., N.C. Romeiro, C.M. Sant'Anna, E.J. Barreiro, and C.A. Fraga, 2009. Structural insights into IKKbeta inhibition by natural products staurosporine and quercetin. Bioorg Med Chem Lett 19: 6907-10.

Barr, I.G., Y.M. Deng, P. Iannello, A.C. Hurt, and N. Komadina, 2008. Adamantane resistance in influenza A(H1) viruses increased in 2007 in South East Asia but decreased in Australia and some other countries. Antiviral Res 80: 200-5.

Barr, I.G., A.C. Hurt, P. Iannello, C. Tomasov, N. Deed, and N. Komadina, 2007. Increased adamantane resistance in influenza A(H3) viruses in Australia and neighbouring countries in 2005. Antiviral Res 73: 112-7.

Berendsen, H.J.C., J.P.M. Postma, W.F. Vangunsteren, A. Dinola, and J.R. Haak, 1984. Molecular-Dynamics with Coupling to an External Bath. Journal of Chemical Physics 81: 3684-3690.

Berman, H.M., J. Westbrook, Z. Feng, G. Gilliland, T.N. Bhat, H. Weissig, I.N. Shindyalov, and P.E. Bourne, 2000. The Protein Data Bank. Nucleic Acids Research 28: 235-242.

Bollrath, J., and F.R. Greten, 2009. IKK/NF-kappaB and STAT3 pathways: central signalling hubs in inflammation-mediated tumour promotion and metastasis. EMBO Rep 10: 1314-9.

Brenke, R., D. Kozakov, G.Y. Chuang, D. Beglov, D. Hall, M.R. Landon, C. Mattos, and S. Vajda, 2009. Fragment-based identification of druggable 'hot spots' of proteins using Fourier domain correlation techniques. Bioinformatics 25: 621-7.

Burke, J.R., and J. Strnad, 2002. The catalytic subunits Of I kappa B kinase, IKK-1 and IKK-2, contain non-equivalent active sites when expressed as homodimers. Biochemical and Biophysical Research Communications 293: 1508-1513.

Bussi, G., T. Zykova-Timan, and M. Parrinello, 2009. Isothermal-isobaric molecular dynamics using stochastic velocity rescaling. Journal of Chemical Physics 130: -.

Castrignano, T., P.D. De Meo, D. Cozzetto, I.G. Talamo, and A. Tramontano, 2006. The PMDB Protein Model Database. Nucleic Acids Research 34: D306-D309.

Cerutti, D.S., P.L. Freddolino, R.E. Duke, and D.A. Case, 2010. Simulations of a Protein Crystal with a High Resolution X-ray Structure: Evaluation of Force Fields and Water Models. Journal of Physical Chemistry B 114: 12811-12824.

Chen, V.B., W.B. Arendall, J.J. Headd, D.A. Keedy, R.M. Immormino, G.J. Kapral, L.W. Murray, J.S. Richardson, and D.C. Richardson, 2010. MolProbity: all-atom structure validation for macromolecular crystallography. Acta Crystallographica Section D-Biological Crystallography 66: 12-21.

Chu, W.M., D. Ostertag, Z.W. Li, L. Chang, Y. Chen, Y. Hu, B. Williams, J. Perrault, and M. Karin, 1999. JNK2 and IKKbeta are required for activating the innate response to viral infection. Immunity 11: 721-31.

Darwech, I., J.E. Otero, M.A. Alhawagri, and Y. Abu-Amer, 2010a. Tyrosine phosphorylation is required for IkappaB kinase-beta (IKKbeta) activation and function in osteoclastogenesis. J Biol Chem 285: 25522-30.

Darwech, I., J.E. Otero, M.A. Alhawagri, and Y. Abu-Amer, 2010b. Tyrosine Phosphorylation Is Required for I kappa B Kinase-beta (IKK beta) Activation and Function in Osteoclastogenesis. Journal of Biological Chemistry 285: 25522-25530.

Daura, X., K. Gademann, B. Jaun, D. Seebach, W.F. van Gunsteren, and A.E. Mark, 1999. Peptide folding: When simulation meets experiment. Angewandte Chemie-International Edition 38: 236-240.

Debondt, H.L., J. Rosenblatt, J. Jancarik, H.D. Jones, D.O. Morgan, and S.H. Kim, 1993. Crystal-Structure of Cyclin-Dependent Kinase-2. Nature 363: 595-602.

Delhase, M., M. Hayakawa, Y. Chen, and M. Karin, 1999. Positive and negative regulation of I kappa B kinase activity through IKK beta subunit phosphorylation. Science 284: 309-313.

DePaul, A.J., E.J. Thompson, S.S. Patel, K. Haldeman, and E.J. Sorin, 2010. Equilibrium conformational dynamics in an RNA tetraloop from massively parallel molecular dynamics. Nucleic Acids Research 38: 4856-4867.

DiDonato, J.A., M. Hayakawa, D.M. Rothwarf, E. Zandi, and M. Karin, 1997. A cytokine-responsive IkappaB kinase that activates the transcription factor NF-kappaB. Nature 388: 548-54.

Duan, Y., C. Wu, S. Chowdhury, M.C. Lee, G.M. Xiong, W. Zhang, R. Yang, P. Cieplak, R. Luo, T. Lee, J. Caldwell, J.M. Wang, and P. Kollman, 2003. A point-charge force field for molecular mechanics simulations of proteins based on condensed-phase quantum mechanical calculations. Journal of Computational Chemistry 24: 1999-2012.

Dupradeau, F.Y., A. Pigache, T. Zaffran, C. Savineau, R. Lelong, N. Grivel, D. Lelong, W. Rosanski, and P. Cieplak, 2010. The R.ED. tools: advances in RESP and ESP charge derivation and force field library building. Physical Chemistry Chemical Physics 12: 7821-7839.

Eswar, N., D. Eramian, B. Webb, M.Y. Shen, and A. Sali, 2008. Protein structure modeling with MODELLER. Methods Mol Biol 426: 145-59.

Fiser, A., and A. Sali, 2003. MODELLER: Generation and refinement of homology-based protein structure models. Macromolecular Crystallography, Pt D 374: 461-+.

Guex, N., M.C. Peitsch, and T. Schwede, 2009. Automated comparative protein structure modeling with SWISS-MODEL and Swiss-PdbViewer: a historical perspective. Electrophoresis 30 Suppl 1: S162-73.

Gupta, S., D. Young, R.K. Maitra, A. Gupta, Z.B. Popovic, S.L. Yong, A. Mahajan, Q. Wang, and S. Sen, 2008. Prevention of cardiac hypertrophy and heart failure by silencing of NF-kappa B. Journal of Molecular Biology 375: 637-649.

Handel, A., I.M. Longini, Jr., and R. Antia, 2007. Neuraminidase inhibitor resistance in influenza: assessing the danger of its generation and spread. PLoS Comput Biol 3: e240.

Hanks, S.K., and T. Hunter, 1995. Protein Kinases .6. The Eukaryotic Protein-Kinase Superfamily - Kinase (Catalytic) Domain-Structure and Classification. Faseb Journal 9: 576-596.

Henikoff, S., and J.G. Henikoff, 1992. Amino-Acid Substitution Matrices from Protein Blocks. Proceedings of the National Academy of Sciences of the United States of America 89: 10915-10919.

Hernandez, L., S.C. Hsu, B. Davidson, M.J. Birrer, E.C. Kohn, and C.M. Annunziata, 2010. Activation of NF-kappaB signaling by inhibitor of NF-kappaB kinase beta increases aggressiveness of ovarian cancer. Cancer Res 70: 4005-14.

Hess, B., H. Bekker, H.J.C. Berendsen, and J.G.E.M. Fraaije, 1997. LINCS: A linear constraint solver for molecular simulations. Journal of Computational Chemistry 18: 1463-1472.

Hess, B., C. Kutzner, D. van der Spoel, and E. Lindahl, 2008. GROMACS 4: Algorithms for highly efficient, load-balanced, and scalable molecular simulation. Journal of Chemical Theory and Computation 4: 435-447.

Hildebrand, A., M. Remmert, A. Biegert, and J. Soding, 2009. Fast and accurate automatic structure prediction with HHpred. Proteins-Structure Function and Bioinformatics 77: 128-132.

Huang, W.C., J.J. Chen, and C.C. Chen, 2003. c-Src-dependent tyrosine phosphorylation of IKKbeta is involved in tumor necrosis factor-alpha-induced intercellular adhesion molecule-1 expression. J Biol Chem 278: 9944-52.

Hubbard, S.R., L. Wei, L. Elis, and W.A. Hendrickson, 1994. Crystal-Structure of the Tyrosine Kinase Domain of the Human Insulin-Receptor. Nature 372: 746-754.

Humphrey, W., A. Dalke, and K. Schulten, 1996. VMD: Visual molecular dynamics. Journal of Molecular Graphics 14: 33-&.

Huse, M., and J. Kuriyan, 2002. The conformational plasticity of protein kinases. Cell 109: 275-282.

Jain, E., A. Bairoch, S. Duvaud, I. Phan, N. Redaschi, B.E. Suzek, M.J. Martin, P. McGarvey, and E. Gasteiger, 2009. Infrastructure for the life sciences: design and implementation of the UniProt website. Bmc Bioinformatics 10: -.

Jeffrey, P.D., A.A. Ruso, K. Polyak, E. Gibbs, J. Hurwitz, J. Massague, and N.P. Pavletich, 1995. Mechanism of Cdk Activation Revealed by the Structure of a Cyclina-Cdk2 Complex. Nature 376: 313-320.

Karin, M., and F.R. Greten, 2005. NF-kappaB: linking inflammation and immunity to cancer development and progression. Nat Rev Immunol 5: 749-59.

Keedy, D.A., C.J. Williams, J.J. Headd, W.B. Arendall, V.B. Chen, G.J. Kapral, R.A. Gillespie, J.N. Block, A. Zemla, D.C. Richardson, and J.S. Richardson, 2009. The other 90% of the protein: Assessment beyond the C alpha s for CASP8 template-based and high-accuracy models. Proteins-Structure Function and Bioinformatics 77: 29-49.

Konia, M.R., S. Schaefer, and H. Liu, 2009. Nuclear factor-kappa B inhibition provides additional protection against ischaemia/reperfusion injury in delayed sevoflurane preconditioning. European Journal of Anaesthesiology 26: 496-503.

Krappmann, D., E.N. Hatada, S. Tegethoff, J. Li, A. Klippel, K. Giese, P.A. Baeuerle, and C. Scheidereit, 2000. The I kappa B kinase (IKK) complex is tripartite and contains IKK gamma but not IKAP as a regular component. Journal of Biological Chemistry 275: 29779-29787.

Lallena, M.J., M.T. Diaz-Meco, G. Bren, C.V. Paya, and J. Moscat, 1999. Activation of IkappaB kinase beta by protein kinase C isoforms. Mol Cell Biol 19: 2180-8.

Landon, M.R., R.L. Lieberman, Q.Q. Hoang, S. Ju, J.M. Caaveiro, S.D. Orwig, D. Kozakov, R. Brenke, G.Y. Chuang, D. Beglov, S. Vajda, G.A. Petsko, and D. Ringe, 2009. Detection of ligand binding hot spots on protein surfaces via fragment-based methods: application to DJ-1 and glucocerebrosidase. J Comput Aided Mol Des.

Lauria, A., M. Ippolito, M. Fazzari, M. Tutone, F. Di Blasi, F. Mingoia, and A.M. Almerico, 2010. IKK-beta inhibitors: An analysis of drug-receptor interactions by using molecular docking and pharmacophore 3-D-QSAR approaches. Journal of Molecular Graphics and Modelling: in press.

Li, Y.Q., A. Roy, and Y. Zhang, 2009. HAAD: A Quick Algorithm for Accurate Prediction of Hydrogen Atoms in Protein Structures. Plos One 4: -.

Lovell, S.C., I.W. Davis, W.B. Arendall, 3rd, P.I. de Bakker, J.M. Word, M.G. Prisant, J.S. Richardson, and D.C. Richardson, 2003. Structure validation by Calpha geometry: phi,psi and Cbeta deviation. Proteins 50: 437-50.

Ludwig, S., and O. Planz, 2008. Influenza viruses and the NF-kappaB signaling pathway - towards a novel concept of antiviral therapy. Biol Chem 389: 1307-12.

Lushington, G.H., 2008. Comparative modeling of proteins, in: A. Kukol, (Ed.), Molecular modeling of proteins, Humana Press, Totowa.

Mahoney, M.W., and W.L. Jorgensen, 2000. A five-site model for liquid water and the reproduction of the density anomaly by rigid, nonpolarizable potential functions. Journal of Chemical Physics 112: 8910-8922.

Mathialagan, S., G.I. Poda, R.G. Kurumbail, S.R. Selness, T. Hall, B.A. Reitz, R.A. Weinberg, N. Kishore, and G. Mbalaviele, 2010. Expression, purification and functional characterization of IkappaB kinase-2 (IKK-2) mutants. Protein Expr Purif 72: 254-61.

Mazur, I., W.J. Wurzer, C. Ehrhardt, S. Pleschka, P. Puthavathana, T. Silberzahn, T. Wolff, O. Planz, and S. Ludwig, 2007. Acetylsalicylic acid (ASA) blocks influenza virus propagation via its NF-kappa B-inhibiting activity. Cellular Microbiology 9: 1683-1694.

Mercurio, F., H. Zhu, B.W. Murray, A. Shevchenko, B.L. Bennett, J. Li, D.B. Young, M. Barbosa, M. Mann, A. Manning, and A. Rao, 1997. IKK-1 and IKK-2: cytokine-activated IkappaB kinases essential for NF-kappaB activation. Science 278: 860-6.

Miyamoto, S., and P.A. Kollman, 1992. Settle - an Analytical Version of the Shake and Rattle Algorithm for Rigid Water Models. Journal of Computational Chemistry 13: 952-962.

Nagarajan, S., H. Choo, Y.S. Cho, K.S. Oh, B.H. Lee, K.J. Shin, and A.N. Pae, IKKbeta inhibitors identification part II: ligand and structure-based virtual screening. Bioorg Med Chem 18: 3951-60.

Nederveen, A.J., and A.M.J.J. Bonvin, 2005. NMR relaxation and internal dynamics of ubiquitin from a 0.2 mu s MD simulation. Journal of Chemical Theory and Computation 1: 363-374.

Ponder, J.W., and D.A. Case, 2003. Force fields for protein simulations. Advances in Protein Chemistry 66: 27-85.

Rockey, W.M., and A.H. Elcock, 2006. Structure selection for protein kinase docking and virtual screening: Homology models or crystal structures? Current Protein & Peptide Science 7: 437-457.

Sali, A., and T.L. Blundell, 1993. Comparative Protein Modeling by Satisfaction of Spatial Restraints. Journal of Molecular Biology 234: 779-815.

Sanner, M.F., 1999. Python: A programming language for software integration and development. Journal of Molecular Graphics & Modelling 17: 57-61.

Sanner, M.F., A.J. Olson, and J.C. Spehner, 1996. Reduced surface: An efficient way to compute molecular surfaces. Biopolymers 38: 305-320.

Schmid, J.A., and A. Birbach, 2008. IkappaB kinase beta (IKKbeta/IKK2/IKBKB)--a key molecule in signaling to the transcription factor NF-kappaB. Cytokine Growth Factor Rev 19: 157-65.

Shen, M.Y., and A. Sali, 2006. Statistical potential for assessment and prediction of protein structures. Protein Science 15: 2507-2524.

Sorin, E.J., and V.S. Pande, 2005. Exploring the helix-coil transition via all-atom equilibrium ensemble simulations. Biophysical Journal 88: 2472-2493.

Sun, W., Y. Yu, G. Dotti, T. Shen, X. Tan, B. Savoldo, A.K. Pass, M. Chu, D. Zhang, X. Lu, S. Fu, X. Lin, and J. Yang, 2009. PPM1A and PPM1B act as IKKbeta phosphatases to terminate TNFalpha-induced IKKbeta-NF-kappaB activation. Cell Signal 21: 95-102.

Wallace, A.C., R.A. Laskowski, and J.M. Thornton, 1995. Ligplot - a Program to Generate Schematic Diagrams of Protein Ligand Interactions. Protein Engineering 8: 127-134.

Wang, J.M., W. Wang, P.A. Kollman, and D.A. Case, 2006. Automatic atom type and bond type perception in molecular mechanical calculations. Journal of Molecular Graphics & Modelling 25: 247-260.

Waterhouse, A.M., J.B. Procter, D.M.A. Martin, M. Clamp, and G.J. Barton, 2009. Jalview Version 2-a multiple sequence alignment editor and analysis workbench. Bioinformatics 25: 1189-1191.

Word, J.M., S.C. Lovell, J.S. Richardson, and D.C. Richardson, 1999. Asparagine and glutamine: Using hydrogen atom contacts in the choice of side-chain amide orientation. Journal of Molecular Biology 285: 1735-1747.

Woronicz, J.D., X. Gao, Z. Cao, M. Rothe, and D.V. Goeddel, 1997. IkappaB kinase-beta: NF-kappaB activation and complex formation with IkappaB kinase-alpha and NIK. Science 278: 866-9.

Yen, H.L., E. Hoffmann, G. Taylor, C. Scholtissek, A.S. Monto, R.G. Webster, and E.A. Govorkova, 2006. Importance of neuraminidase active-site residues to the neuraminidase inhibitor resistance of influenza viruses. J Virol 80: 8787-95.

Yin, M.J., Y. Yamamoto, and R.B. Gaynor, 1998. The anti-inflammatory agents aspirin and salicylate inhibit the activity of I(kappa)B kinase-beta. Nature 396: 77-80.

Tables

Table 1: Assessment results for comparative models and templates

Model	DOPE z-score	MolProbity score	Ramachandran plot[1]	
			a	**b**
IKK-β (Modeller)	-0.388	3.08	91.92%	1.68%
IKK-β (SAMD)	-0.779	0.98	92.09%	1.08%
1RDQE	-1.80	1.25	97.59%	0.00%
3G51A	-1.73	1.50	98.10%	0.00%
3HKOA	-1.28	1.77	96.99%	0.00%
3DTC	- 1.43	3.19	90.67%	1.78%
1ZY4A	-1.57	2.08	96.84%	0.40%
3FE3A	-1.55	2.60	96.04%	0.33%
1PHKA	-1.54	2.87	94.68%	0.76%

[1] **a**, Ramachandran favored; **b**, Ramachandran outliers

Table 2: Cluster analyis of the MD trajectory between 10 ns and 80 ns

Cluster	fraction of trajectory[1]	RMSD[2] /nm
ATP1	74.0 %	0.57
ATP2	24.3 %	0.39
ATP3	1.6 %	0.47
noATP1	83.5 %	0.46
noATP2	13.1 %	0.35
noATP3	1.6 %	0.48
noATP4	1.3 %	0.56

[1] The fraction of the trajectory during which the protein adopts are particular structure within an RMSD cut off of 0.2 nm. Only clusters with a fraction larger than 1% are shown

[2] RMSD with respect to the final comparative model

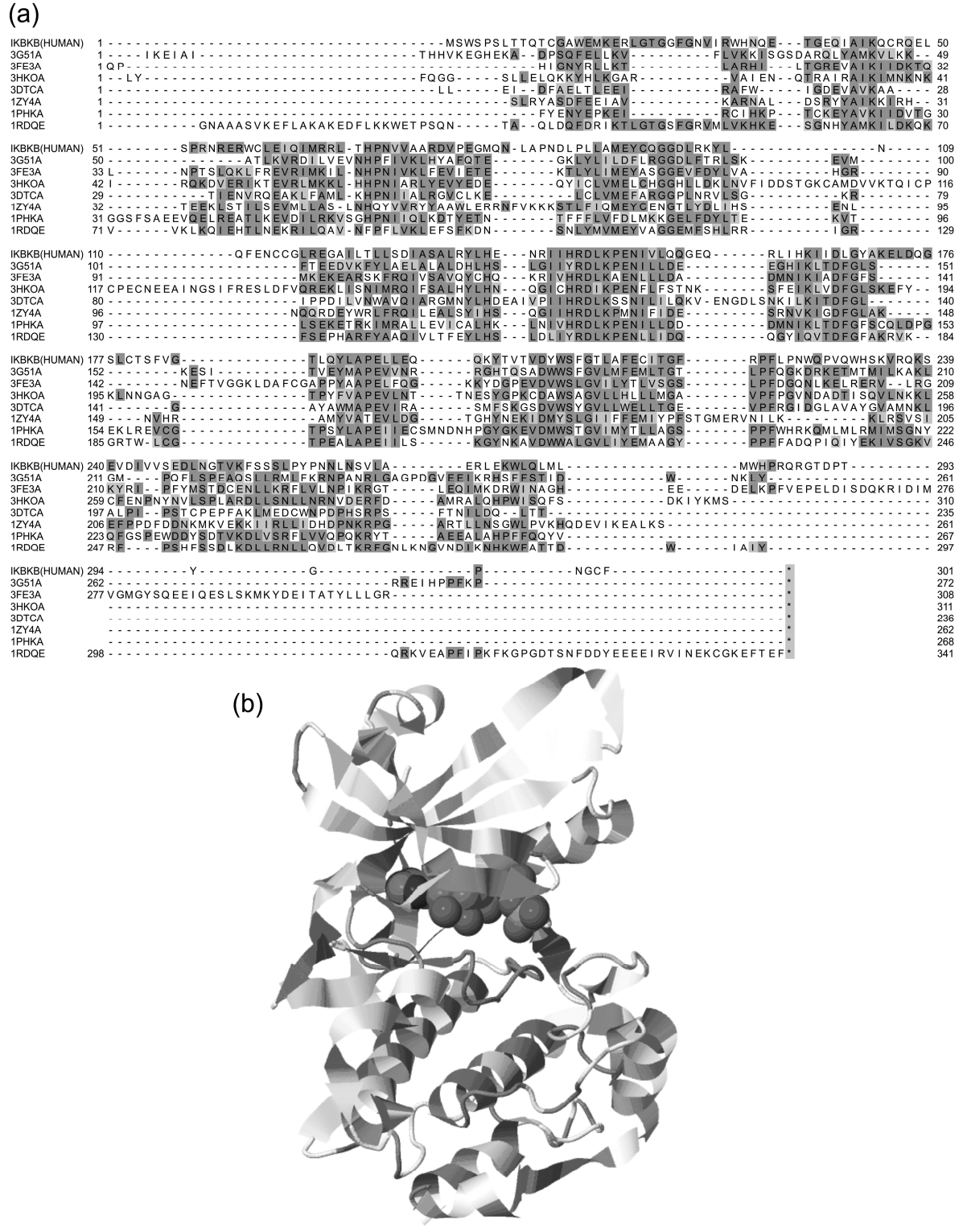

Figure 1: (a) Multiple sequence alignment of the IKK-β kinase domain (IKBKB Human) with the sequences of structural templates used for comparative modelling. The sequences are shaded according to similarity using the BLOSUM62 score. (b) 3D backbone structure of the initial IKK-β model shaded according to similarity with any one of the templates. This figure was made with Jalview (Waterhouse et al., 2009).

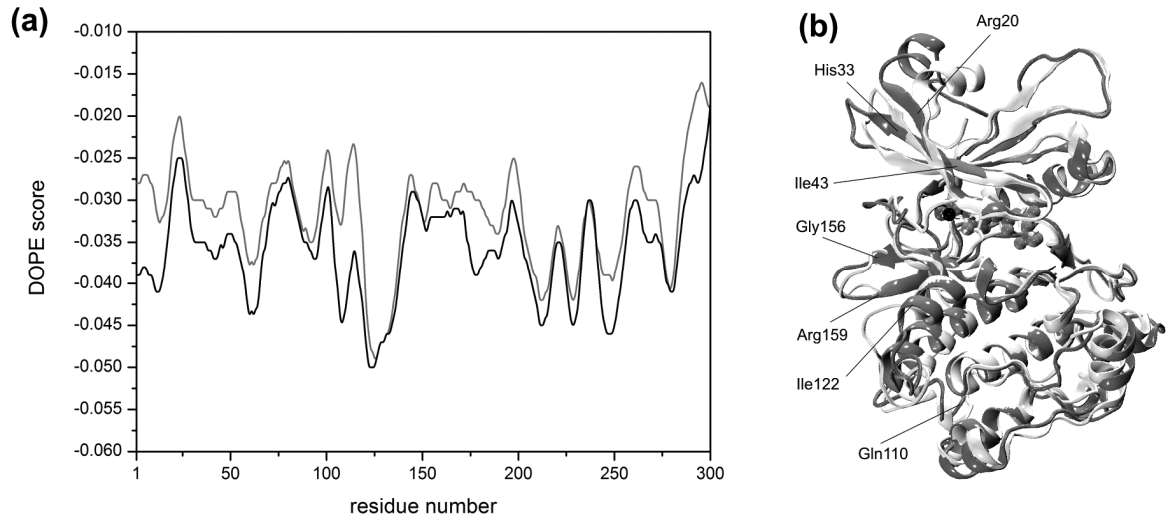

Figure 2: (a) Profile of the per-residue DOPE model assessment score of the initial model (grey curve) and final SAMD model (black curve). (b) Superposition of the 3D backbone structure of the final SAMD model (blue) with the initial model (white). This figure was made with VMD (Humphrey et al., 1996).

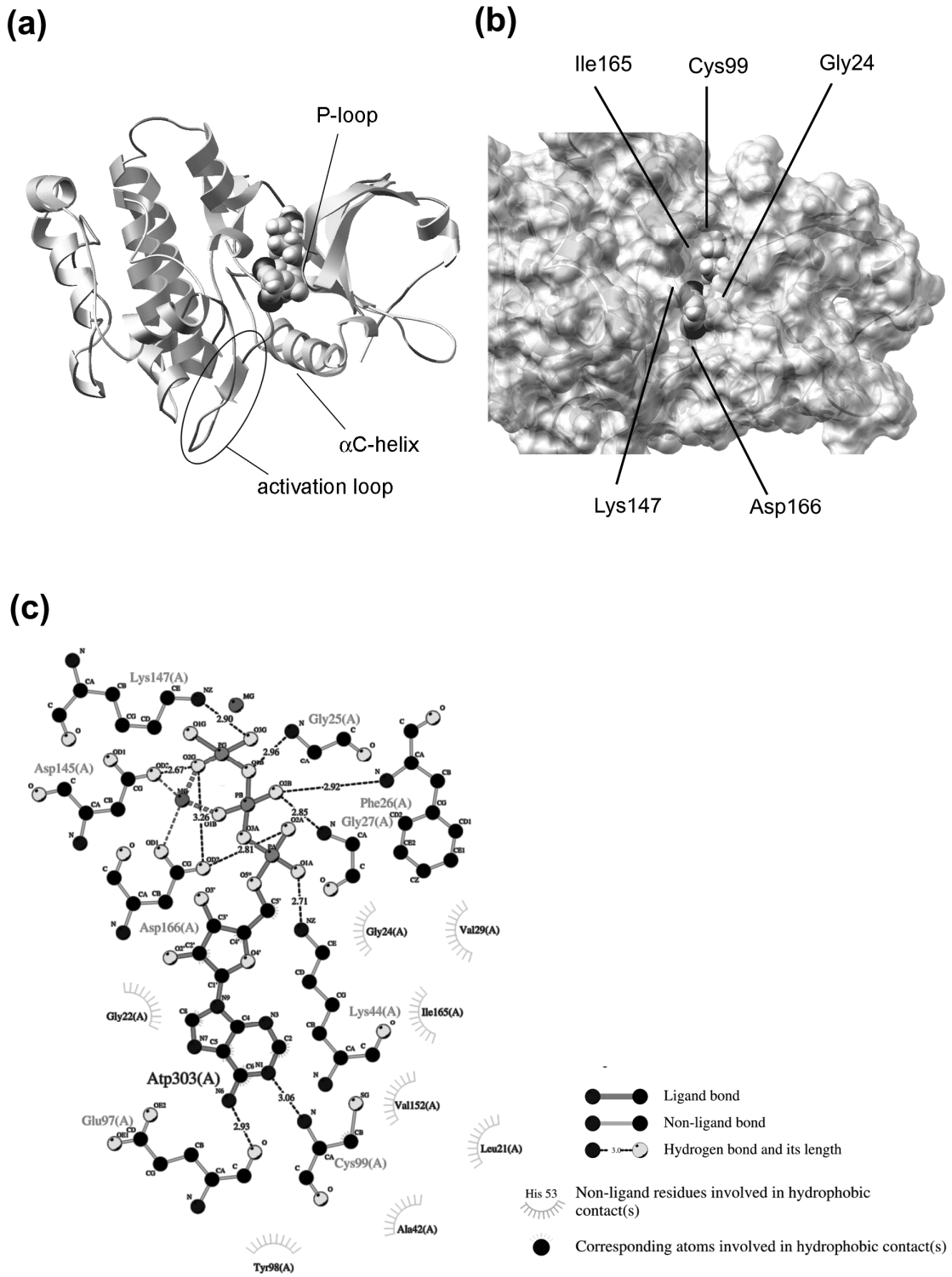

Figure 3: (a) Backbone representation the final IKK-β model with ATP in Van der Waals representation. (b) Solvent accessible surface representation of IKK-β with ATP in van der Waals representation, a selection of interacting amino acid residues are highlighted. This figure was made with Python Molecular Viewer(Sanner, 1999; Sanner et al., 1996). (c) 2D representation of the ATP-protein interaction. Bonds within the ATP ligand are shown in purple. This figure was made with LigPlot (Wallace et al., 1995).

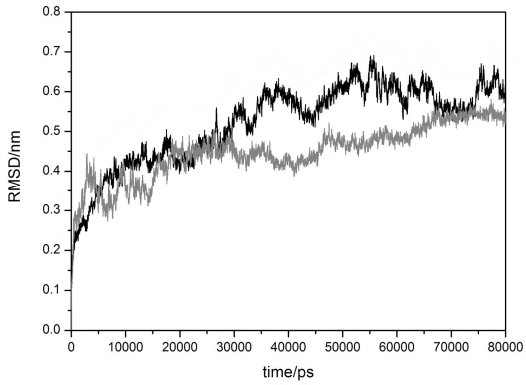

Figure 4: Root mean square deviation (RMSD) of the backbone coordinates with respect to the final model is shown for IKK-β with ATP/Mg bound (black curve) and without ATP (grey curve) plotted against MD simulation time.

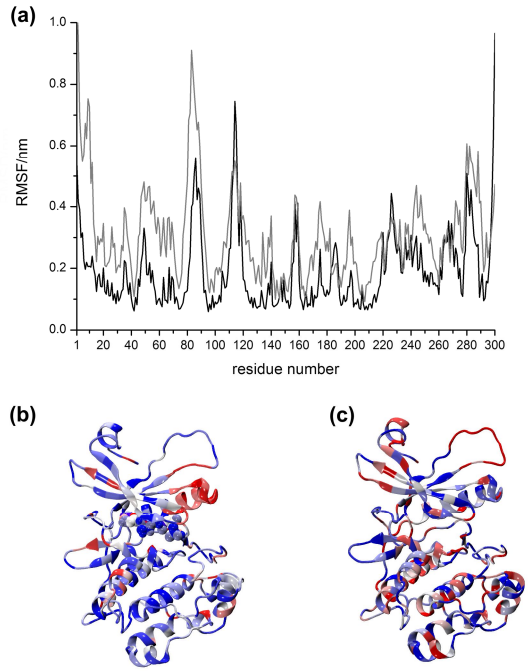

Figure 5: (a) Root mean square fluctuations (RMSF) averaged over all atoms of an amino acid residue plotted against the residue number for IKK-β with ATP/Mg bound (black curve) and without ATP (grey curve). (b) The protein backbone structure of IKK-β with ATP coloured according to the root mean square fluctuations of backbone atoms from blue (low fluctuations) to red (high fluctuations). (c) The representation for IKK-β without ATP.

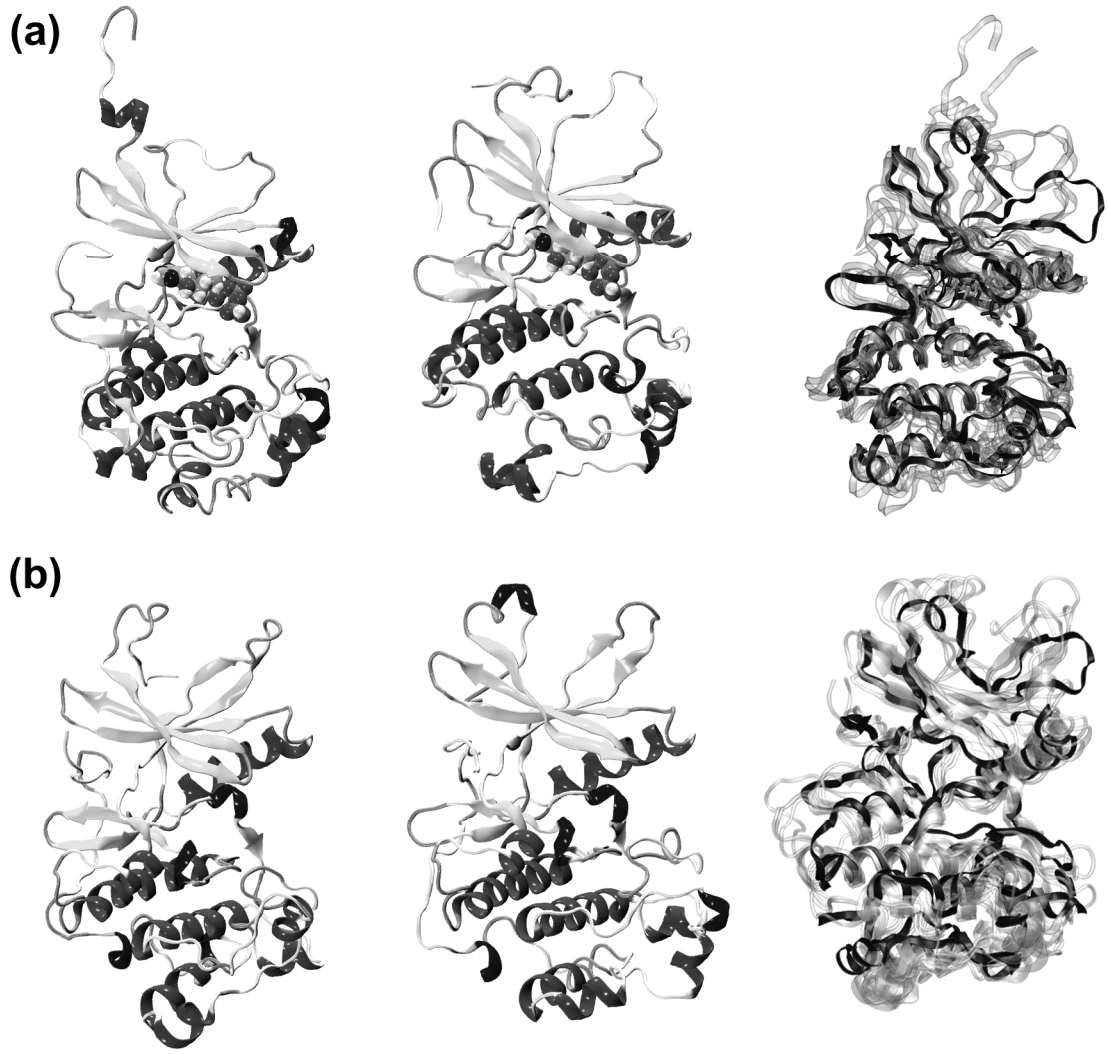

Figure 6: The two major conformations adopted by IKK- β from left to right ATP1 and ATP2 (a) and noATP1, no ATP2 (b). Additionally an overlay of all conformations in table 2 with the final comparative model is shown.

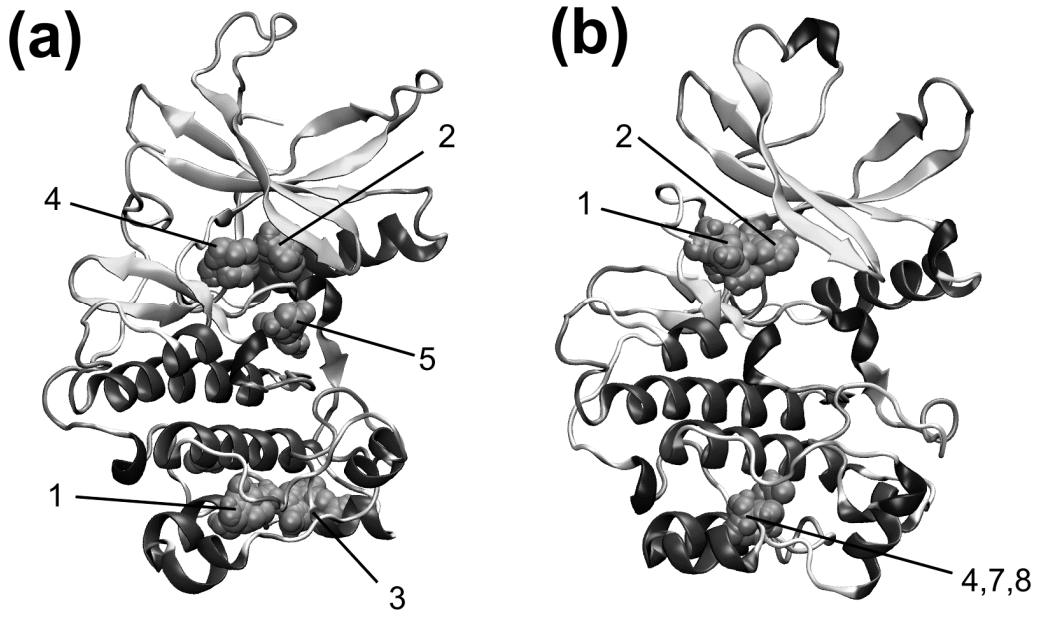

Figure 7: Binding site analysis with the FTmap (Brenke et al., 2009) algorithm of the two major conformations without ATP co-factor, (a) noATP1 and (b) noATP2. The numbers show the ranking of binding sites with one being the highest rank.